Phosphoregulation in the N-terminus of NRT2.1 affects nitrate uptake by controlling the interaction of NRT2.1 with NAR2.1 and kinase HPCAL1

Zhi Li, Na Xu, Aurore Jaquot, Valentin Chaput, Mattia Adamo, Benajmin Neuhäuser, Tatsiana Straub, Laurence Lejay, Waltraud X Schulze

Phosphoregulation in the N-terminus of NRT2.1 affects nitrate uptake by controlling the interaction of NRT2.1 with NAR2.1 and kinase HPCAL1

Zhi Li [1,4], Xu Na Wu [1,5], Aurore Jaquot [2], Valentin Chaput [2], Mattia Adamo [2], Benajmin Neuhäuser [3], Tatsiana Straub [1], Laurence Lejay [2], Waltraud X Schulze [1]

[1] Department of Plant Systems Biology, University of Hohenheim, 70593, Stuttgart, Germany

[2] BPMP, University Montpellier, CNRS, INRAE, Montpellier SupAgro, Montpellier, France

[3] Department of Crop Physiology, University of Hohenheim, 70593, Stuttgart, Germany

[4] Current Department of Biology, University of North Carolina at Chapel Hill, Chapel Hill, NC 27599, USA

[5] Current State Key Laboratory of Conservation and Utilization of Bio-Resources in Yunnan and Center for Life Science, School of Life Sciences, Yunnan University, Kunming, China

Address for correspondence:

Prof. Waltraud Schulze

Department of Plant Systems Biology

University of Hohenheim

70599 Stuttgart, Germany

wschulze@uni-hohenheim.de

Highlight

Major plant nitrate uptake transporter NRT2.1 is activated by phosphorylation at either serine S28 or S21. Receptor kinase HPCAL1 was identified as involved in phosphorylation of NRT2.1 at serine S21.

Abstract

NRT2.1, the major high affinity nitrate transporter in roots, can be phosphorylated at five different sites within N- and C-terminus. Here, we characterized the functional relationship of two N-terminal phosphorylation sites, S21 and S28. Based on a site-specific correlation network we identified a receptor kinase (HPCAL1, AT5G49770), phosphorylating NRT2.1 at S21 and resulting in active nitrate uptake. HPCAL1 itself was regulated by phosphorylation at S839 and S870 within its kinase domain. In the active state, when S839 was dephosphorylated and S870 was phosphorylated, HPCAL1 was found to interact with the N-terminus of NRT2.1, mainly when S28 was dephosphorylated. Phosphorylation of NRT2.1 at S21 resulted in a reduced interaction of NRT2.1 with its activator NAR2.1, but nitrate transport activity remained. By contrast, phosphorylated NRT2.1 at S28 enhanced the interaction with NAR2.1, but reduced the interaction with HPCAL1. HPCAL1 here was identified as the kinase affecting this phospho-switch through phosphorylation of NRT2.1 at S21.

Keywords

Nitrate transporter NRT2.1, posttranslational regulation, protein phosphorylation, kinase HPCAL1, nitrate, plasma membrane

Introduction

For most plants growing in temperate regions, nitrate is the main form of nitrogen taken up from the soil, which is mediated by members of the NRT2 and NPF protein families (Leran *et al.*, 2014). The uptake of nitrate through dedicated transporters was under study for a long time (Krapp *et al.*, 2014), and has identified several nitrate transporters in roots as well as in green tissue (Kiba *et al.*, 2012). These nitrate transporters are classified into two major groups based on their uptake modes as a low affinity transport system or a high affinity transport system (Wang *et al.*, 2012).

NRT2.1 (AT1G08090) is the major high affinity nitrate transporter in Arabidopsis roots as shown by the loss of 75% of HATS activity in *nrt2.1* knock-out mutants (Cerezo *et al.*, 2001). A strong correlation between root nitrate influx and *NRT2.1* gene expression was observed (Girin *et al.*, 2007; Lejay *et al.*, 1999), leading to the conclusion that transcriptional regulation of NRT2.1 is a key mechanism to control nitrate uptake. Consequently, regulation of NRT2.1 in the past was mainly studied at gene transcriptional level. *NRT2.1* gene expression is induced upon nitrate (Lejay *et al.*, 1999) and repressed by high nitrogen metabolism and high external nitrate concentrations (Girin *et al.*, 2007; Lejay *et al.*, 1999). By contrast, *NRT2.1* gene expression was up-regulated by light and sugars (Lejay *et al.*, 2003; Lejay *et al.*, 1999) and is affected by the C/N status of the plant (Girin *et al.*, 2007; Krouk *et al.*, 2010). Further, reciprocal regulation of NRT2.1 and ammonium transporters by nitrate and ammonium influx was described (Camanes *et al.*, 2012; Gansel *et al.*, 2001).

NRT2.1 is regulated by protein-protein interaction with a small single-transmembrane protein, NAR2.1 (AT5G50200) (Laugier *et al.*, 2012; Orsel *et al.*, 2007). Both proteins need to be present in the plasma membrane to result in full nitrate uptake activity (Orsel *et al.*, 2006). In addition, *nar2.1* mutants seem to be defective in trafficking of NRT2.1 to the plasma membrane (Wirth *et al.*, 2007). NAR2.1 was proposed to form a hetero-oligomer with NRT2.1 (Yong *et al.*, 2010), but the precise mechanism by which this complex forms remains unclear. Furthermore, abundance of NRT2.1 protein within the membrane remains rather constant despite measurable changes in HATS activity upon stimulation by high nitrate, sugars, or light (Laugier *et al.*, 2012; Wirth *et al.*, 2007). This points to tight control of NRT2.1 activity by posttranslational modifications. Posttranslational control of nitrate transport activity is well described for dual-affinity transporter NRT1.1 (AT1G12110) (Guo *et al.*, 2001; Liu *et al.*, 1999). In NRT1.1, phosphorylation at threonine 101 acts as a switch. When T101 is phosphorylated, NRT1.1 functions as high affinity transporter. When T101 is dephosphorylated, NRT1.1 functions as low affinity transporter (Liu and Tsay, 2003). This affinity switch by phosphorylation has recently been related to conformational changes of NRT1.1 (Parker and Newstead, 2014). CIPK23 (AT1G30270) was identified as a kinase phosphorylating NRT1.1 at T101 (Ho *et al.*, 2009).

With accumulation of global (phospho)proteomics data sets acquired under nitrate stimulation (Engelsberger and Schulze, 2012; Wang *et al.*, 2013) or nitrate deprivation (Menz *et al.*, 2016), several phosphorylation sites for NRT2.1 were identified. However, functional consequence of NRT2.1 N-terminal phosphorylation is yet unclear, and the respective kinases and phosphatases remain uncharacterized. Here, we studied NRT2.1 posttranslational modification status under different conditions of nitrate availability. We aimed to identify kinases that might exert posttranslational control of the major nitrate uptake transporter NRT2.1.

Materials and Methods

Experimental design – Two phosphoproteomics data sets were used to study NRT2.1 phosphorylation and reconstruct kinase-substrate networks. Firstly, we used a previously published nitrate deprivation data set (Supplementary Figure S1A) in which plants were grown in hydroponic culture at 3 mM nitrate and then subjected to nitrate deprivation by transferring plants to nitrate-free nutrient solution. Plants were harvested before nitrate starvation (0 minutes), and after 15 minutes and 3 hours of nitrate deprivation (Menz *et al.*, 2016). Secondly, we conducted a nitrate-resupply experiment (Supplementary Figure S1B), in which plants were grown at 3 mM nitrate, then starved for nitrate for two days. After starvation, nitrate was resupplied at a concentration of 0.2 mM or 5 mM for 5 and 15 minutes. In all experiments, three to four biological replicates of root tissue were processed for (phospho)proteomic analysis and results are presented as averages with standard deviation. Statistical comparisons were carried out by pairwise t-tests (two sample comparisons) or ONEWAY ANOVA (multiple sample comparisons).

Plant material – Experiments were performed with *Arabidopsis thaliana* wild type (Col-0) and the homozygous knock-out mutants *nrt2.1* (SALK_035429) and *at5g49770* (SALK_068035) with T-DNA insertion into promoter region. No AT5G49770 protein was detected in the knock-out line.

Constructs – Constructs were made using Gateway technology. For ratiometric bimolecular Fluorescence Complementation (rBiFC) of Arabidopsis proteins, cDNAs of the following genes were cloned into rBiFC plasmids (Grefen and Blatt, 2012): AT5G49770 without and with phosphorylation site mutations at T792, S839, S870, S919, and NRT2.1 without and with phosphorylation site mutations at S11, S21 and S28. Phosphorylation sites were mutated either to alanine (mimicking no phosphorylation) or aspartate (putative phosphorylation mimic). For purification of cytoplasmic domain of AT5G49770 to be used in *in vitro* kinase assays, the cytoplasmic domain (amino acids 583 to 946) was cloned into *Escherichia coli* BL21(DE3) expression plasmid pET-21a(+) and fused with His-tag (plasmid AT5G49770CD-HIS). Cytoplasmic domains of two homologs AT5G49760 (HPCA1/CARD1) and AT5G49780 were also used.

In vitro kinase activity assay – Plasmids expressing kinase domains with and without phosphorylation site mutations were transferred into *Escherichia coli* BL21(DE3). After induction with isopropyl ß-D-thiogalactopyranoside, cells were harvested and lysed using BugBuster Protein Extraction Reagent (Novagen, Nottingham, UK), expressed proteins were purified over gravity flow Ni^{2+}-NTA sepharose (IBA GmbH, Goettingen, Germany). In vitro kinase assays were performed using the ADP-Glo™ Kinase assay kit (Promega, Germany) with minor modifications. Kinase (cytoplasmic domain, 1nmol) was incubated with 5 µg substrate in kinase reaction buffer (40mM Tris-HCl, pH 7.5, 1mM $MgCl_2$, 0,01 % BSA, 50 µM NaF, 1 µM $Na3VO_3$, 1mM $CaCl_2$, 100 µM ATP, 1 mM DTT). As generic kinase substrate myelin basic protein was used in the kinase reaction buffer. After incubation for one hour, 30 µl ADP-GLO Reagents (Promega, Germany) was added and incubated for 40 minutes. Then, Kinase Detection Reagents were added and incubated for another hour. Luminescence as a measure of ATP conversion from ADP was recorded with a luminometer (Tecan M200 Pro). Specific NRT2.1 substrate peptides were obtained from a QconCAT artificial protein consisting of concatenated tryptic peptides around NRT2.1 phosphorylation sites. After incubation at room temperature for 1 hour, the reaction was terminated by heating at 90°C for 10 minutes. Phosphopeptides were collected at the end of the kinase reaction over titanium dioxide.

Ratiometric bimolecular fluorescence assay – Ratiometric bimolecular florescence complementation (rBiFC) assays were conducted in transiently transformed *Nicotiana benthamiana* using a Zeiss LSM700 confocal microscope (Wu *et al.*, 2019b). All images were collected using exactly the same settings. YFP and RFP intensity was measured using the FIJI software (Schindelin *et al.*, 2012) and YFP/RFP ratios was calculated. 10- 50 different cells were analyzed. Statistical significance was determined using pairwise ranksum test. To calibrate YFP/RFP ratios, known interaction of NRT2.1 with NAR2.1 served as reference (Laugier *et al.*, 2012).

Nitrate influx assay – Root NO_3^- influx was assayed as described previously (Laugier *et al.*, 2012). Plants were sequentially transferred to 0.1 mM $CaSO_4$ for 1 minute, to a complete nutrient solution, pH 5.8, containing 0.2mM $^{15}NO_3$ (99 atom % excess ^{15}N) for 5 minutes, and finally to 0.1mM $CaSO_4$ for 1 minute. Roots were then separated from shoots, and the roots dried at 70 °C for 48 h. After determination of their dry weight, samples were analyzed for total nitrogen and atom % ^{15}N using a continuous flow isotope ratio mass spectrometer coupled with a C/N elemental analyzer (ANCA-MS; PDZ Europa, Crewe, UK). Each influx value is the mean of 6 to 12 replicates.

Gene expression analysis – Root samples were frozen in liquid N_2 in 2 mL tubes containing one steel bead (2.5 mm diameter). Tissues were disrupted for 1 min at 28 s^{-1} in a mixer mill homogenizer (MM301, Retsch, Germany). Total RNA was extracted from tissues using Trizol reagent (Invitrogen, Carlsbad, CA, USA). Subsequently, 4 µg of RNA were treated with DNase I (Amplification Grade, Sigma-Aldrich) following the manufacturer's instructions. Reverse transcription was achieved with 4 µg of RNA in the presence of Moloney Murine Leukemia Virus reverse transcriptase (RNase H minus, Point Mutant, Promega) after annealing with an anchored oligo$(dT)_{18}$ primer as described (Wirth *et al.*, 2007). Quality of the cDNA was verified by PCR using specific primers spanning an intron in gene APTR (At1g27450) forward 5'-CGCTTCTTCTCGACACTGAG-3'; reverse 5'-CAGGTAGCTTCTTGGGCTTC-3'.

Gene expression was determined by quantitative real-time PCR (LightCycler 480, Roche Diagnostics) using the SYBRR Premix Ex TaqTM (TaKaRa) according to the manufacturer's instructions with 1 µl of cDNA in a total volume of 10 µl. All expression values were standardized to *Clathrin* (*At4g24550*). Gene-specific primer sequences were: *NRT2.1* forward, 5'-AACAAGGGCTAACGTGGATG-3'; *NRT2.1* reverse, 5'-CTGCTTCTCCTGCTCATTCC-3'; *NAR2.1* forward, 5'-GGCCATGAAGTTGCCTATG -3'; *NAR2.1* reverse, 5'- TCTTGGCCTTCCTCTTCTCA -3'; *Clathrin* forward, 5'-AGCATACACTGCGTGCAAAG-3'; *Clathrin* reverse, 5'-TCGCCTGTGTCACATATCTC-3'. *At5g49770* forward 5'-CCAACCGTAACTTGAAAGGAAAGC-3' *At5g49770* reverse 5'-TCAGGATTGCCAGTCAAATCCAAG-3'. We selected the gene clathrin (At4g24550) as a control gene based on its lack of regulation by the conditions we are studying. It was independently identified as a suitable reference gene for nutrient experiments in a large-scale survey of 1400 possible reference genes across a wide range of conditions (Czechowski *et al.*, 2004).

Microsomal protein and phosphopeptide enrichment – A total of 1 to 1.5 g of root fresh weight was homogenized in 10 ml ice-cold extraction buffer (330 mM mannitol, 100 mM KCl, 1 mM EDTA, 50 mM Tris-MES, fresh 5 mM DTT, and 1 mM phenylmethylsulfonylfluoride, pH 7.5) (Pertl *et al.*, 2001) in the presence of 0.5 % v/v proteinase inhibitor mixture (Sigma-Aldrich, Germany) and phosphatase inhibitors (25 mM NaF, 1 mM Na_3VO_4, 1 mM benzamidin, 3 µM proteinase inhibitor leupeptin). The homogenate was centrifuged for 15 minutes at 7500 × g at 4°C. The pellet was discarded, and the

supernatant was centrifuged for 75 minutes at 48,000 × g at 4°C. Microsomal pellets were stored at -80°C until further processing. Microsomal pellets were resuspended in 100 µl of membrane buffer (330 mM mannitol, 25 mM Tris-MES, 0.5 mM DTT) or UTU (6 M urea, 2 M thiourea, pH 8). Further tryptic digestion, desalting over C_{18} and enrichment of phosphopeptides over titanium dioxide beads was performed as described (Wu *et al.*, 2017).

LC-MS/MS analysis of peptides – Peptides mixtures were analyzed by nanoflow Easy-nLC (Thermo Scientific) and Orbitrap hybrid mass spectrometer (Q-Exactive, Thermo Scientific) as described previously (Tan *et al.*, 2022; Wu *et al.*, 2019b). Proteins were identified based on information-dependent acquisition of fragmentation spectra of multiple charged peptides. MaxQuant version 1.5.3.8 (Cox and Mann, 2008) was used for raw file peak extraction and protein identification against the TAIR10 database (35386 entries). Protein quantification was performed in MaxQuant using label free quantification algorithm (Cox *et al.*, 2014). The following parameters were applied: trypsin as cleaving enzyme; minimum peptide length of seven amino acids; maximal two missed cleavages; carbamidomethylation of cysteine as a fixed modification; N-terminal protein acetylation, oxidation of methionine as variable modifications. For phosphopeptide identification, phosphorylation of serine, threonine, and tyrosine was included as variable modifications. Mass tolerances were used as in MaxQuant default settings: 4.5 ppm for precursor ions and 20ppm as MS/MS tolerance. Further settings were: "label-free quantification" marked, multiplicity set to 1; "match between runs" marked with time window 0.7 minutes; peptide and protein false discovery rates (FDR) set to 0.01; common contaminants (trypsin, keratin, etc.) excluded. The raw MS data from this study was deposited at the ProteomeXchange Consortium (http://proteomecentral.proteomexchange.org) via the PRIDE partner repository with the identifier PXD015390 for nitrate starvation data set, and PXD014146 for nitrate resupply data set.

Statistical analyses and data visualization – Phosphosites ion intensity data were extracted from evidence.txt, log_2-transformed and normalized using Perseus (Tyanova *et al.*, 2016). Briefly, phosphosites quantified in at least 50 % of the biological replicates were analyzed by ANOVA. Other statistical analyses were carried out with Sigma Plot (version 11.0) and Excel (version 2013). Over-representation analysis was done by Fisher's exact test, p values were adjusted by Bonferroni correction. Functional classification of proteins was done based on MAPMAN (Thimm *et al.*, 2004). Information about subcellular location was derived from SUBA3 (Tanz *et al.*, 2013). Detailed protein function was manually updated with the support of TAIR (Huala *et al.*, 2001). Published protein-protein interactions were retrieved from STRING (Franceschini *et al.*, 2013).

Results

This work is based on two large-scale phosphoproteomics data sets of wild type roots describing phosphorylation events induced by nitrate deprivation (Menz *et al.*, 2016) (Supplementary Figure S1A), and nitrate resupply (Supplementary Figure S1B). The mass spectrometry raw data of these two experimental sets were jointly processed and quantified. In the combined data set, 4746 phosphopeptides were identified (Supplementary Table S1), and at least one quantitative value was obtained for 4670 phosphopeptides. Nitrate deprivation and nitrate resupply affected phosphorylation of diverse proteins at the plasma membrane, particularly the phosphorylation of H^+-ATPases (bin 34.1), and aquaporins (bin 34.19), which were down-regulated (dephosphorylated) by nitrate-starvation and up-regulated (phosphorylated) by nitrate resupply. Proteins of protein synthesis (bin 29.2.1) and various signaling pathways through receptor kinases (bin 30.2) and

calcium (bin 30.3) were also affected by both nitrate treatments. Proteins in glycolysis (bin 4.1) were only affected by nitrate deprivation (Supplementary Figure S1C), while proteins of nitrate assimilation (bin 12.1.1) were increased in phosphorylation by nitrate resupply (Supplementary Figure S1C).

NRT2.1 was found to be phosphorylated at different sites in the N- and C-terminus, namely at S11 ((ac)GDSTGEPGSS(ph)MHGVTGR), S28 (EQSFAFSVQS(ph)PIVHTDK), S501 (NMHQGS(ph)LR), and T521 (SAAT(ph)PPENTPNNV) with distinct phosphopeptide intensities at nitrate starvation or nitrate resupply. Phosphorylation at S28 was quantified already in previous starvation-resupply experiments (Engelsberger and Schulze, 2012). The phosphopeptides corresponding to phosphorylation at S11, S28, S501 and T521 sites were also identified in independent nitrate nutrition experiments (Jacquot *et al.*, 2020). Phosphorylation at S21 with peptide EQS(ph)FAFSVQSPIVHTDK (Supplementary Figure S2, Supplementary Table S1) has not been explicitly described previously, and was identified by careful re-analysis of nitrate deprivation data sets (Menz *et al.*, 2016).

NRT2.1 activity is regulated by N-terminal phosphorylation

To understand the role of N-terminal phosphorylation sites for the activity of NRT2.1, site directed mutants of NRT2.1 were created, in which major phosphorylation sites were mutated to a putative phosphomimicking aspartate (D), or phosphodead alanine (A). These site-directed NRT2.1 mutants were expressed under *NRT2.1* promoter in *nrt2.1* knock-out background. Nitrate influx was measured for nitrate starved plants, as well as for plants after nitrate induction with 1 mM nitrate for 1 and 4 hours. In wild type, higher nitrate influx was measured after 4 hours of induction compared to nitrate influx rates of roots starved for nitrogen. In *nrt2.1-2* knock-out mutant, no induction of nitrate uptake was observed by 1 mM nitrate treatment, resulting in significantly lower nitrate uptake than in wild type after 4 hours of induction (Figure 1). Phosphorylation site mutations at NRT2.1 S11 resulted in wild-type like influx of $^{15}NO_3^-$ under all conditions in the phosphodead S11A mutant, while nitrate influx was significantly reduced in phosphomimicking S11D mutants, although influx rates remained still higher than in *nrt2.1* knock-out mutant (Figure 1A). This suggests that phosphorylation of NRT2.1 at S11 down-regulates nitrate influx. For phosphorylation site mutations at S28 we observed a significantly reduced nitrate influx for S28A mutants similar to *nrt2.1* knock-out mutant, and wild-type like nitrate influx for phosphomimicking mutation S28D (Figure 1B). This suggests that phosphorylation of NRT2.1 at S28 activates nitrate influx directly or stabilizes NRT2.1 protein turnover. For newly discovered phosphorylation site S21, we also found reduced nitrate influx activity for plants with phosphodead S21A (Figure 1C), while for plants with phosphomimicking S21D, averaged nitrate influx activity was higher than in plant lines with S21A after 4 hours of 1 mM nitrate resupply. This suggests that phosphorylation at S21 also leads to a higher activity of NRT2.1.

Phosphorylation-dependent NRT2.1 regulation through interaction with NAR2.1

Nitrate transporter NRT2.1 is regulated by the interaction with protein NAR2.1 (Laugier *et al.*, 2012,Orsel, 2006 #2553; Orsel *et al.*, 2007). Therefore, we used ratiometric bimolecular fluorescence complementation (Grefen and Blatt, 2012) to explore whether the interaction of NRT2.1 with NAR2.1 was affected by NRT2.1 phosphorylation (Figure 2A, Supplementary Figure S3). The confirmed interaction of NRT2.1 with NAR2.1 was used as a reference. There was no difference between phosphomimic mutation (S11D) and phosphodead mutations (S11A) for S11. For S21 we

observed a significantly increased interaction of NAR2.1 with phosphodead S21A compared to the phosphomimicking S21D, which displayed a weaker interaction with NAR2.1. By contrast, NRT2.1 with phosphomimicking S28D displayed stronger interaction with NAR2.1 than NRT2.1 with phosphodead mutation S28A. Interestingly, however, if both phosphorylation sites were mutated together to create mimic of a singly phosphorylated NRT2.1 N-terminus (S21A/S28D, S21D/S28A), NAR2.1 showed strong interactions with both versions and highest interaction with the version phosphomimicking S28D. This suggests a single phosphosite in the N-terminus is sufficient for interaction of NRT2.1 and NAR2.1, but S28 is the preferred site. Since the *in vivo* phosphorylation status of NRT2.1 in singly mutated constructs (Figure 2A) remains unknown, the doubly phospho-mutated version (Figure 2B) give more precise insights.

Identification of kinases phosphorylating NRT2.1

Based on existing nitrate starvation and nitrate resupply data sets (Engelsberger and Schulze, 2012; Menz *et al.*, 2016), and with addition of data from new resupply-experiments with 0.2mM and 5 mM nitrate, we aimed to identify kinases acting on the different phosphorylation sites of NRT2.1. Many kinases are subject to regulation by phosphorylation (Zulawski and Schulze, 2015), suggesting that kinases phosphorylating NRT2.1 are likely also to be regulated by nitrate-dependent phosphorylation. Thus, we expected phosphorylation profiles of a kinase and its substrate to be highly correlated under conditions when phosphorylation of kinase and substrates both have activating, or both have inactivating effects. Alternatively, phosphorylation of a kinase and its substrates are expected to be anti-correlated if one activating and one inactivating phosphorylation occurs. To identify such kinase candidates, phosphorylation profiles of NRT2.1 phosphorylation sites S11, S28, S501 and T521 were correlated with phosphorylation profiles of identified kinases (Supplementary Figure S4, Supplementary Table S2). NRT2.1 phosphorylation site S21 was not included due to low data coverage across conditions. Following this approach, phosphorylation profile correlation pairs were strictly filtered based on their correlation r-value ($r > 0.9$ or $r < -0.9$). As a result, 12 protein kinases were identified only under nitrate deprivation, 30 protein kinases were identified only under nitrate resupply conditions (5 mM NO_3 or 0.2 mM NO_3) and 9 protein kinase were identified under nitrate depletion as well as under nitrate resupply (Figure 3A, Supplementary Table 2).

Kinases with phosphorylation profiles highly correlated with NRT2.1 phosphorylation included MAPKKK7 (AT3G13530), for which phosphorylation positively correlated with phosphorylation of NRT2.1 at S11 and T521. Phosphorylation of CIPK25 (AT5G25110) correlated with NRT2.1 phosphorylation at S11, phosphorylation of CALCIUM-DEPENDENT PROTEIN KINASE 29 (CPK29, AT1G76040) was correlated with phosphorylation at T521. Phosphorylation of CDPK19 (AT5G19450) and MAP4K4 (AT5G14720) at different sites were connected to the phosphorylation profiles of NRT2.1 at S11, S28, and S501. Among the receptor kinases, phosphorylation of BAM1 (AT5G65700) positively correlated with S11 and S501 phosphorylation, and phosphorylation of PHYTOSULFOKINE RECEPTOR 1 (PSKR1, AT2G02220) correlated with NRT2.1 phosphorylation at S501. C-terminal phosphorylation at LIEEVSHSSGS(ph)PNPVS(ph)D of co-receptor QSK1 (AT3G02880) showed a negative correlation with phosphorylation at S28 and T521. Phosphorylation of kinase AT5G49770 at S839 showed positive correlation with NRT2.1 phosphorylation at S28 under low nitrate supply (Supplementary Table S2). Receptor kinase AT5G49770 raised our further interest, since four phosphorylation sites were identified within the activation loop at T792 (LVGDPEKAHVT(ph)TQVK),

in the kinase domain at S839 (SPIDRGS(ph)YVVK) and S870 (NLYDLQELLDTTIIQNS(ph)GNLKGFEK), and within disordered C-terminal region at S919 (LVGLNPNADS(ph)ATYEEASGDPYGR) (Supplementary Figure S5).

The phosphorylation network was further complemented with known interaction partners of NRT2.1 and kinase candidate AT5G49770 as retrieved from public sources (Franceschini *et al.*, 2013) (Figure 3B). Thereby, it became obvious that NRT2.1 was shown to interact with several other kinases besides AT5G49770, among them VIK1 (AT1G14000) (Wingenter *et al.*, 2011), a MAP kinase (AT3G46930), phytosulfokine receptor kinase PSKR1 (AT2G02220), and several uncharacterized receptor kinases (Figure 3B). By contrast, kinase AT5G49770 had been found to interact with various other transport proteins within the membrane besides NRT2.1, for example with H^+-ATPases AHA1 (AT2G18960) and AHA2 (AT4G30190), and several members of the ABC transporter family (PGP6 AT2G39480, PGP19 AT3G28860, PDR7 AT1G15210, PGP4 AT2G47000, PGP11 AT1G02520, MRP10 AT3G62700, PGP20 AT3G55320). Furthermore, kinase AT5G49770 connected to the calcium signaling pathway through interactions with CPK29 (AT1G76040), CPK7 (AT5G12480), CPK6 (AT2G17290), and CBL3 (AT4G26570). A connection to nitrate assimilation was found through interaction of AT5G49770 with nitrate reductases NIA2 (AT1G37130) and NIA1 (AT1G77760).

Kinase AT5G49770 interacts with and phosphorylates NRT2.1

Kinase candidate AT5G49770 was then tested for its ability to interact with NRT2.1 *in planta*, and we further tested whether this interaction was affected by the phosphorylation status of the kinase. Indeed, we showed an interaction of AT5G49770 with NRT2.1 in the ratiometric bimolecular fluorescence complementation system (Figure 4A, Supplementary Figure S6A). Phosphorylation site mutations of AT5G49770 at sites T792, S870 and S919 did not affect the interaction with NRT2.1. However, when S839 was mutated to alanine, interaction of AT5G49770 S839A with NRT2.1 was significantly increased compared to AT5G49770 S839D, when S839 was mutated to phosphomimicking aspartate. Thus, interaction of AT5G49770 with NRT2.1 was stronger when S839 was dephosphorylated. Next, we explored NRT2.1 as substrate for kinase AT5G49770 (Figure 4B). The intracellular domain of AT5G49770 was recombinantly expressed (Supplementary Figure S7) and exposed to the substrate peptide EQSFAFSVQSPIVHTDK in *in-vitro* kinase assays (Wu and Schulze, 2015). Indeed, kinase domain of AT5G49770 was able to phosphorylate the substrate peptide at S21. Significantly higher NRT2.1S21 phosphorylation was observed from kinase domains with phosphodead mutation S839A. By contrast, phosphomimicking mutation S839D yielded lower substrate phosphorylation at NRT2.1S21 compared to AT5G49770S839A, but still higher kinase activities than in wild type. Also, mutations at S870 lead to differential substrate phosphorylation efficiency: phosphomimicking mutation AT5G49770S870D resulted in higher kinase activity towards NRT2.1 N-terminal peptide than phosphodead mutation AT5G49770S870A. No significant difference in substrate phosphorylation between phosphomimicking and phosphodead versions of recombinant kinase domain were observed for other phosphorylation sites in AT5G49770 (Figure 4B). Consistently, all *in vitro* kinase activity assays showed substrate phosphorylation only at the serine corresponding to NRT2.1 S21 (Figure 4C), and never at the site corresponding to S28 or the double phosphorylated forms.

Interestingly, when generic kinase substrate myelin basic protein was used in the in-vitro kinase assay instead of specific NRT2.1 substrate peptide, phosphorylation site mutations at S839 did not

result in differential kinase activity, and increased kinase activity was only observed for AT5G49770S870D mutation (Figure 4D). These results suggest that phosphorylation of AT5G49770 at S870 regulated general kinase activity (towards a generic substrate), while phosphorylation of AT5G49770 at S839 rather affected interaction with the specific substrate. Indeed, when S839 was phosphorylated (phosphomimicked S839D), interaction of AT5G49770 with NRT2.1 was reduced (Figure 4A) and lower levels of substrate phosphorylation at S21 occurred (Figure 4B). When S870 was phosphorylated (phosphomimicked S870D), kinase activity generally was enhanced (Figure 4D), there was higher phosphorylation activity towards the NRT2.1 S21 peptide, but overall interaction of AT5G49770 with NRT2.1 was not significantly affected (Figure 4A).

We then checked *in-planta* phosphorylation status of NRT2.1 and AT5G49770 (Figure 5) in the two nitrogen nutrition experiments, namely nitrogen deprivation for 15 minutes and 3 hours (Menz *et al.*, 2016), and nitrate starvation resupply experiment with two days of nitrate starvation followed by resupply of either 0.2 mM or 5 mM nitrate for 5 minutes or 15 minutes. NRT2.1S21 tended to be increasingly phosphorylated at nitrate resupply with high (5 mM) nitrate, but not under prolonged nitrate starvation for 2 days (Figure 5A). By contrast, NRT2.1S28 phosphorylated under nitrate starvation and low nitrate supply and showed a trend for dephosphorylation at high nitrate concentrations (5 mM) (Figure 5B). This confirmed published observations of NRT2.1S28 dephosphorylation upon 3mM nitrate resupply (Engelsberger and Schulze, 2012). Kinase AT5G49770 was found with increasing phosphorylation at S870 after resupply of 5 mM nitrate (Figure 5C) dephosphorylation at S839 (Figure 5D). Other phosphorylation sites of AT5G49770 were only detected at very low levels under nitrogen starvation and resupply with low (0.2 mM) nitrate (Figure 5E). In summary, NRT2.1 phosphorylation at S21 and S28 showed a tendency for anti-correlation at high nitrate supply: When S21 was highly phosphorylated, phosphorylation at S28 was detected at lower level and *vice versa* (Figure 5A, B). A similar anti-correlation was also observed for S839 and S870 of kinase AT5G49770 (Figure 5C, D).

Nitrate uptake in kinase mutant at5g49770

Interaction of kinase AT5G49770 with NRT2.1 in bimolecular fluorescence complementation assays was found to be affected by NRT2.1 phosphorylation status at S28 (Figure 5F, Supplementary Figure S6B). AT5G49770 showed significantly weaker interactions with NRT2.1 in phosphorylation mimicking NRT2.1S28D mutant compared to phosphodead NRT2.1S28A. This suggests that interaction of kinase AT5G49770 with NRT2.1 is not favored by phosphorylation at S28 (Figure 5F). Testing the interaction of AT5G49770 with the double-mutated NRT2.1 confirmed reduced interaction of the kinase with NRT2.1 S28D and stronger interaction of the kinase with the NRT2.1 S21D (Supplementary Figure S6C). The interaction of AT5G49770 with NRT2.1 mutated at S11 remained largely unaffected (Figure 5F).

In the knock-out mutant *at5G49770* we observed a significantly higher nitrate influx than in *nrt2.1* knock out (Figure 6A), reaching wild type like nitrate influx rates upon nitrate induction (1 mM NO_3^- for 4 or 7h). Thus, in absence of AT5G49770, nitrate influx was high, consistent with high activity of NRT2.1. We therefore propose that under 1mM nitrate supply, in the absence of AT5G49770, NRT2.1 may remain in the highly active complex together with NAR2.1 when S28 is phosphorylated. The active state observed when AT5G49770 showed highest interaction with NRT2.1, i.e. when S28 is dephosphorylated, may occur under specific cellular conditions. It may not be the dominant state

of NRT2.1 and could be a transition state to fine-tune NRT2.1 activity status. Kinase AT5G49770 was recently named HPCAL1, as a homolog of H_2O_2-receptor HPCA1 (Wu *et al.*, 2020) and/or as a quinone receptor CARD1 (Laohavisit *et al.*, 2020). The observed uptake rates in *hpcal1* (*at5g49770*) knock-out mutant were consistent with unaltered *NRT2.1* mRNA abundance in the mutant (Figure 6B). However, a reduced expression of *NAR2.1* mRNA was observed in the kinase mutant *at5g49770* (Figure 6B), suggesting possibility for downstream signaling effects. Expression of *AT5g49770* was not dependent on presence of NRT2.1, since *nrt2.1* mutant showed similar levels of *Hpcal1* (*At5g49770*) mRNA as wild type, at least under the conditions tested here (Figure 6B).

Since phosphorylation of NRT2.1 at S28 was also shown to affect NRT2.1 stability (Zou *et al.*, 2019), we analyzed NRT2.1 protein abundance under conditions of 4h nitrate induction used for nitrate influx assays. The abundance of NRT2.1 was significantly reduced in transgenic plants bearing phosphodead NRT2.1S28A (Supplementary Figure S8A). This confirms stabilization of NRT2.1 by phosphorylation at S28 (Zou *et al.*, 2019). Protein abundance of NAR2.1 (Supplementary Figure S8B) as well as protein abundance of kinase HPLCAL1 (Supplementary Figure S8C) was not affected by phosphorylation site mutations of NRT2.1 at S21 or S28.

Discussion

There are (at least) five phosphorylation sites which differentially affect nitrate uptake of nitrate transporter NRT2.1. In the C-terminus, phosphorylation of S501 was recently shown to result in inactivation of NRT2.1 without affecting the interaction of NRT2.1 with NAR2.1 (Jacquot *et al.*, 2020). In the N-terminus, phosphorylation (or phosphomimic) of S28 mediated high nitrate uptake, while phosphorylation at S11 resulted in low nitrate uptake. Phosphorylation at S28 was shown to stabilize NRT2.1 at the plasma membrane (Zou *et al.*, 2019), but may additionally lead to direct regulation by affecting interactions with NAR2.1. The molecular mechanisms by which this posttranslational control at these different sites takes effect, can be very different for each of these sites. Interestingly, dephosphorylation at S11 enhanced NRT2.1 transport activity, but interaction with NAR2.1 was not affected by phosphorylation state at S11. This indicates that transport activity of NRT2.1 may require further regulation even when NRT2.1 interacted with NAR2.1. The main discovery in our study is that single phosphorylation of NRT2.1 at either S21 or S28 results in active nitrate influx, and that HCAL1 is the kinase involved in NRT2.1 phosphorylation at S21. Interestingly, kinase HPCAL1 was also proposed to interact with nitrate transporters (also NRT1.1) in size-exclusion chromatography coupled to mass spectrometry approach, separating protein complexes and reconstructing their interaction network (Gilbert *et al.*, 2021; Gilbert and Schulze, 2019).

It is well known that phosphorylation of the same protein at different sites, or different modifications at closely neighboring sites can influence the nature of protein-protein interactions and consequently the activity of proteins or signaling pathways. Recently, in plant receptor kinase signaling, a tyrosine phosphorylation switch has been discovered in BAK1/SERK3 which in the phosphorylated state activates immune signaling, and in dephosphorylated state feeds into other signaling pathways (Perraki *et al.*, 2018). Also, multisite phosphorylation in ribosomal protein S6 kinase 1 (S6K1) was shown to alter substrate specificity of the kinase (Arif *et al.*, 2018). Phosphorylation of three different sites at S6K1 was required for it to phosphorylate one substrate but not the other. Here, we present an example in which phosphorylation at spatially closely neighboring serine residues in the N-terminus of NRT2.1 resulted in preferred recruitment of

different interaction partners, either NAR2.1 or kinase HPCAL1 to these particular sites. Currently, it cannot be excluded that trimeric complexes exist, and it is also likely that the interaction status of individual NRT2.1 molecules could be in different interaction states, leading to a mixture of complexes. Nitrogen status and the resulting phosphorylation status of NRT2.1 likely determine the dominant complex form of NRT2.1 and thus the resulting uptake rates.

Regulation of transporters at the plasma membrane by multiple phosphorylation sites, as described here for NRT2.1, could well be a general principle, particularly for proteins that are under control of many different signals. For example, the H^+-ATPase AHA2 is regulated by two different activating phosphorylation sites in its C-terminus and by at least one inactivating phosphorylation site in one cytosolic loop (Rudashevskaya *et al.*, 2012). In addition, these regulatory phosphorylation sites of AHA2 are targeted by different kinases which control proton flux in response to different stimuli (Caesar *et al.*, 2011; Fuglsang *et al.*, 2003; Fuglsang *et al.*, 2014; Haruta *et al.*, 2015; Haruta *et al.*, 2008). A role in fine-tuning of transporter activity was recently also proposed for a series of serine phosphorylation sites in the C-terminus of the ammonium transporter family (Wu *et al.*, 2019a).

Functional model of the NRT2.1 phospho-regulation at S21/S28

NRT2.1 here was found to be phosphorylated with several sites at N- and C-terminus. At the same time, the regulatory pattern of NRT2.1 turned out to be very complex and under transcriptional and posttranscriptional control of external nitrate supply as well as the metabolic C/N status of the plant (Camanes *et al.*, 2012; Gansel *et al.*, 2001; Li *et al.*, 2016; Wirth *et al.*, 2007). Therefore, it is of no surprise to find highly complex regulatory mechanisms involving phosphorylation sites in the N-terminus to add to the multifactorial control of NRT2.1 activity at the protein level. NRT2.1 is active mainly at low nitrate conditions (e.g. 0.2 mM to 1mM). Under these conditions, the NRT2.1 was found highly phosphorylated at S28 and showed strong interactions with activator NAR2.1 (Figure 7A). At low nitrate, HPCAL1 was found phosphorylated at S839, and in this state shows reduced interaction with NRT2.1. Most likely, HPCAL1 under these conditions is dephosphorylated at S870, corresponding to a less active kinase domain (Figure 5 C, D).

Under resupply of higher external nitrate (3 to 5 mM) NRT2.1 phosphorylation at S28 was reduced. This results in decreased protein stability (Zou *et al.*, 2019), but also slightly enhances the interaction with receptor kinase HPCAL1 (Figure 2). HPCAL1 – dephosphorylated at S839 and activated by (auto)phosphorylation at S870 (Figure 5) – can then interact with and phosphorylate NRT2.1 at S21 and switch it into an active state (Figure 7B). In this active state NRT2.1 can still interact with NAR2.1 (Figure 2B).

The double-phosphorylated state of NRT2.1 (Supplementary Figure S9) was experimentally only found transiently after nitrate resupply. In this state (Figure 7C), the interaction with activator NAR2.1 was found to be weak (Figure 2B), and uptake rates were lower (Supplementary Figure S10). It could likely present a fast mechanism to (temporarily) reduce nitrate influx. Such a (temporary) reduction in nitrate influx could be useful for the plant under limiting carbon availability and/or when sufficient amino acids have been built in the assimilation pathway (Girin *et al.*, 2010; Lejay *et al.*, 1999). The doubly-dephosphorylated state (Figure 7D) is considered as instable at the plasma membrane (Supplementary Figure S8A, (Zou *et al.*, 2019)) and may thus have a higher turnover. However, interaction of NRT2.1S21AS28A with activator NAR2.1 potentially remained (Figure 2B). Our findings point to a significant regulation of NRT2.1 activity through phosphorylation events at

S21 and S28. It needs to be kept in mind, however, that phosphoregulation of NRT2.1 at the C-terminus (Jacquot *et al.*, 2020) may overlay the measured effects described here.

We suggest kinase HPCAL1 to function in switching instable, double dephosphorylated NRT2.1 to an active state by with phosphorylation of S21 (Figure 7D). In addition, HPCAL1 could also participate in switching NRT2.1 to the more inactive, double-phosphorylated state. When kinase HPCAL1 is absent (in *at5g49770*), NRT2.1 most likely remains stabilized in highly active state phosphorylated at S28 (Figure 7A) and in interaction with NAR2.1.

In support of our regulatory model, singly phosphorylated NRT2.1 (S21AS28D or S21DS28A) showed higher nitrate influx activity than double-dephosphorylated NRT2.1 (S21AS28A) or doubly-phosphorylated NRT2.1 (S21DS28D) (Supplementary Figure S10). Activation of NRT2.1 was recently described to involve a type 2C protein phosphatase (Ohkubo *et al.*, 2021). Although in that study, the action of the phosphatase dephosphorylated NRT2.1 at S501, we expect yet unknown phosphatases to be involved in regulation of NRT2.1 also at the N-terminus.

Phosphoregulation of kinase HPCAL1

Receptor kinase HPCAL1 is highly and almost exclusively expressed in root tissue, particularly in the lateral root cap (Winter *et al.*, 2007) and shows high overlap with NRT2.1 expression. There are two closely related kinases (HPCA1/CARD1, AT5G49760 and HPCAL2, AT5G49780) within the Arabidopsis proteome sharing high homology to our candidate kinase AT5G49770 (Supplementary Figure S10). AT5G49760 was highly expressed in leaf tissue and anthers, with rather low expression values in roots, and AT5G49780 showed moderate general expression also in roots, but at lower levels than AT5G49770 (Winter *et al.*, 2007). The phosphorylation site at S839 was unique to AT5G49770, while in AT5G49760 and AT5G49780 a lysine is present at the respective position within the sequence (Supplementary Figure S10). In the kinase activity assays, AT5G49780 was largely inactive, while AT5G497760 (HPCA1/CARD1) displayed a higher activity towards substrate peptide EQSFAFSVQSPIVHTDK than did AT5G49770. This high activity could possibly be explained by the fact that regulatory phosphorylation site identified for AT5G49770 with S839 was not present in AT5G49760 and therefore this kinase may show constitutively higher activity. We cannot provide clear explanation for the observed inactivity of recombinant kinase domain AT5G49780, possibly this is connected to an additional sequence at amino acids 609 to 629 (Supplementary Figure S10). Despite the orthologs, own proteomic evidence and gene expression patterns (Winter *et al.*, 2007) point to expression of AT5G49770 (HPCAL1) as the dominant isoform in young root tissue which was analyzed here. The expression of AT5G49760 was dominant in leaves.

Protein kinases can be regulated by phosphorylation within their kinase domain. Most prominent examples are mitogen-activated protein kinases (MAP-Kinases), which are activated by double-phosphorylation of a well-conserved TEY motif within the activation loop (Rodriguez *et al.*, 2010). Also in SUCROSE NON-FERMENTING 1-RELATED PROTEIN KINASE 1 (SnRK1), phosphorylation of the kinase domain is required for full activity (Emanuelle *et al.*, 2018). We propose that phosphorylation of HPCAL1 at S870 affects general kinase activity, while phosphorylation at S839 affects interaction with the substrate NRT2.1. Phosphorylation site T792 was predicted (InterPro, (Mitchell *et al.*, 2019)) within the activation loop of the kinase. However, under conditions used in our experiments, mutations of T792 did not affect activity of HPCAL1. There are several kinases in which phosphorylation of activation loop is not required for activation (Nolen *et al.*, 2004). Possibly, in

HPCAL1, steric access to the activation loop and active center is regulated by (de)phosphorylation of S839 rather than by phosphorylation of the activation loop itself. Recent structural analyses of kinase catalytic domains revealed that the activation loop requires N- and C-terminal structural anchors which correctly place the activation loop neighboring the ATP-binding site and catalytic domain (Nolen *et al.*, 2004). In HPCAL1 phosphorylation site S839 is located within a region that could serve as C-terminal anchor for activation loop. However, the precise role of different phosphorylation sites of HPCA1/CARD1-protein family needs to be fully explored in further experiments.

In summary, serines S21 and S28 in the N-terminus of NRT2.1 activate nitrate influx in singly phosphorylation states. HPCAL1 was identified as the kinase phosphorylating and activating NRT2.1 at S21. The interaction of HPCAL1 with NRT2.1 – which was favored when S28 was dephosphorylated – is further fine-tuned by phosphorylation within HPCAL1 at serines S839 and S870. Activity changes of NRT2.1 and effects on high-affinity nitrate transport activity are the final result.

Supplementary data

Supplementary Figure S1: Experimental data sets used in this study.

Supplementary Figure S2: Best spectra of NRT2.1 phosphopeptides directly exported from MaxQuant.

Supplementary Figure S3: Representative images of the interaction of NRT2.1 with NAR2.1.

Supplementary Figure S4: Workflow of identification of protein kinases which might phosphorylate NRT2.1.

Supplementary Figure S5: Best spectra of kinase HPCAL1 phosphopeptides directly exported from MaxQuant.

Supplementary Figure S6: Representative images of the interaction of ratiometric bimolecular fluorescence assays

Supplementary Figure S7: SDS-PAGE gel detection after immobilized metal affinity chromatography (IMAC) purification of the intracellular domain of AT5G49760, AT5G49770, and AT5G49780.

Supplementary Figure S8: Protein abundances under conditions of nitrate uptake for NRT2.1, NAR2.1, Kinase HPCAL1.

Supplementary Figure S9: Doubly phosphorylated peptide of NRT2.1 covering sites S21 and S28.

Supplementary Figure S10: Nitrate influx by NRT2.1 with double phosphorylation site mutations at S21 and S28 at 4 hours of induction by 1mM nitrate.

Supplementary Figure S11: Close homologs of AT5G49770. The proteins AT5G49760 and AT5G49780 are closely related to the candidate kinase AT5G49770.

Supplementary Table 1: Summary of identified phosphopeptides from the joint analysis of nitrate deprivation experiment (Menz *et al.*, 2016) and nitrate starvation – resupply experiment with 0.2 mM and 5 mM nitrate resupply. In both experimental sets, only root material was analyzed. Quantitative values indicate normalized ion intensities (Zauber and Schulze, 2012).

Supplementary Table 2: Correlation network of NRT2.1 N-terminal phosphorylation sites with phosphorylation sites of different kinases under nitrogen deprivation (Menz *et al.*, 2016) and nitrate resupply with 0.2 mM and 5 mM nitrate.

Acknowledgements

We thank Zhaoxia Zhang for help with bioinformatics scripting and Sven Gombos for technical assistance in the lab.

Funding Statement

This work was supported by an international grant from the ANR in France (SIPHON ANR-13-ISV6-0002-01) and Deutsche Forschungsgemeinschaft (SCHU1533/8-1) in Germany.

Author contribution

ZL performed majority of experiments, developed kinase-substrate network screen and contributed to writing; XNW performed rBIFC experiments; AJ, VC, MA, BN performed nitrate uptake experiments and qPCR experiments, TS performed nitrate uptake experiments on double mutants and contributed to writing; LL analyzed data and contributed to writing; WXS analyzed data, designed figures and wrote the manuscript.

Conflict of Interest

Authors declare no conflict of interest.

Data availability

The raw MS data from this study was deposited at the ProteomeXchange Consortium (http://proteomecentral.proteomexchange.org) via the PRIDE partner repository with the identifier PXD015390 for nitrate starvation data set, and PXD014146 for nitrate resupply data set. Supplementary Tables include then network raw data and phosphoproteome lists.

References

Arif A, Jia J, Willard B, Li X, Fox PL. 2018. Multisite Phosphorylation of S6K1 Directs a Kinase Phospho-code that Determines Substrate Selection. *Molecular Cell*.

Caesar K, Elgass K, Chen Z, Huppenberger P, Witthöft J, Schleifenbaum F, Blatt MR, Oecking C, Harter K. 2011. A fast brassinolide-regulated response pathway in the plasma membrane of Arabidopsis thaliana. *Plant Journal* **66**, 528-540.

Camanes G, Bellmunt E, Garcia-Andrade J, Garcia-Agustin P, Cerezo M. 2012. Reciprocal regulation between AtNRT2.1 and AtAMT1.1 expression and the kinetics of NH(4)(+) and NO(3)(-) influxes. *Journal of Plant Physiology* **169**, 268-274.

Cerezo M, Tillard P, Filleur S, Munos S, Daniel-Vedele F, Gojon A. 2001. Major alterations of the regulation of root NO(3)(-) uptake are associated with the mutation of Nrt2.1 and Nrt2.2 genes in Arabidopsis. *Plant Physiology* **127**, 262-271.

Cox J, Hein MY, Luber CA, Paron I, Nagaraj N, Mann M. 2014. Accurate proteome-wide label-free quantification by delayed normalization and maximal peptide ratio extraction, termed MaxLFQ. *Molecular and Cellular Proteomics* **13**, 2513-2526.

Cox J, Mann M. 2008. MaxQuant enables high peptide identification rates, individualized p.p.b.-range mass accuracies and proteome-wide protein quantification. *Nature Biotechnology* **26**, 1367-1372.

Czechowski T, Bari RP, Stitt M, Scheible WR, Udvardi MK. 2004. Real-time RT-PCR profiling of over 1400 Arabidopsis transcription factors: unprecedented sensitivity reveals novel root- and shoot-specific genes. *The Plant Journal* **2004**, 366-379.

Emanuelle S, Doblin MS, Gooley PR, Gentry MS. 2018. The UBA domain of SnRK1 promotes activation and maintains catalytic activity. *Biochemical and Biophysical Research Communications* **497**, 127-132.

Engelsberger WR, Schulze WX. 2012. Nitrate and ammonium lead to distinct global dynamic phosphorylation patterns when resupplied to nitrogen starved Arabidopsis seedlings. *The Plant Journal* **69**, 978-995.

Franceschini A, Szklarczyk D, Frankild S, Kuhn M, Simonovic M, Roth A, Lin J, Minguez P, Bork P, Von Mering C, Jensen LJ. 2013. STRING v9.1: protein-protein interaction networks, with increased coverage and integration. *Nucleic Acids Research* **41**, D808-D815.

Fuglsang AT, Borch J, Bych K, Jahn TP, Roepstorff P, Palmgren MG. 2003. The binding site for regulatory 14-3-3 protein in plant plasma membrane H+-ATPase: involvement of a region promoting phosphorylation-independent interaction in addition to the phosphorylation-dependent C-terminal end. *Journal of Biological Chemistry* **278**, 42266-42272.

Fuglsang AT, Kristensen A, Cuin T, Schulze WX, Persson J, Thuesen KH, Ytting CK, Oehlschlaeger C, Mahmood K, Sondergaard TE, Shabala S, Palmgren MG. 2014. Receptor kinase mediated control of primary active proton pumping at the plasma membrane. *The Plant Journal* **80**, 951-964.

Gansel X, Muños S, Tillard P, Gojon A. 2001. Differential regulation of the NO3 and NH4 transporter genes AtNrt2.1 and AtAmt1.1 in Arabidopsis: relation with long-distance and local controls by N status of the plant. *The Plant Journal* **26**, 143-155.

Gilbert M, Li Z, Wu XN, Rohr L, Gombos S, Harter K, Schulze WX. 2021. Comparison of path-based centrality measures in protein-protein interaction networks revealed proteins with phenotypic relevance during adaptation to changing nitrogen environments. *Journal of Proteomics* **235**, 104114.

Gilbert M, Schulze WX. 2019. Global Identification of Protein Complexes within the Membrane Proteome of Arabidopsis Roots Using a SEC-MS Approach. *Journal of Proteome Research* **18**, 107-119.

Girin T, El-Kafafi e-S, Widiez T, Erban A, Hubberten HM, Kopka J, Höfgen R, Gojon A, Lepetit M. 2010. Identification of Arabidopsis mutants impaired in the systemic regulation of root nitrate uptake by the nitrogen status of the plant. *Plant Physiology* **153**, 1250-1260.

Girin T, Lejay L, Wirth J, Widiez T, Palenchar PM, Nazoa P, Touraine B, Gojon A, Lepetit M. 2007. Identification of a 150bp cis-acting element of the AtNRT2.1 promoter involved in the regulation of gene expression by the N and C status of the plant. *Plant, Cell and Environment* **30**, 1366-1380.
Grefen C, Blatt MR. 2012. A 2in1 cloning system enables ratiometric bimolecular fluorescence complementation (rBiFC). *Biotechniques* **53**, 311-314.
Guo FQ, Wang R, Chen M, Crawford NM. 2001. The Arabidopsis dual-affinity nitrate transporter gene AtNRT1.1 (CHL1) is activated and functions in nascent organ development during vegetative and reproductive growth. *Plant Cell* **13**, 1761-1777.
Haruta M, Gray WM, Sussman MR. 2015. Regulation of the plasma membrane proton pump (H-ATPase) by phosphorylation. *Current Opinion in Plant Biology* **28**, 68-75.
Haruta M, Monshausen G, Gilroy S, Sussman MR. 2008. A cytoplasmic Ca2+ functional assay for identifying and purifying endogenous cell signaling peptides in Arabidopsis seedlings: identification of AtRALF1 peptide. *Biochemistry* **47**, 6311-6321.
Ho C-H, Lin SH, Hu HC, Tsay YF. 2009. CHL1 functions as a nitrate sensor in plants. *Cell* **138**, 1184-1194.
Huala E, Dickerman AW, Garcia-Hernandez M, Weems D, Reiser L, LaFond F, Hanley D, Kiphart D, Zhuang M, Huang W, Mueller LA, Bhattacharyya D, Bhaya D, Sobral BW, Beavis W, Meinke DW, Town CD, Somerville C, Rhee SY. 2001. The Arabidopsis Information Resource (TAIR): a comprehensive database and web-based information retrieval, analysis, and visualization system for a model plant. *Nucleic Acids Research* **29**, 102-105.
Jacquot A, Chaput V, Mauries A, Li Z, Tillard P, Fizames C, Bonillo P, Bellegarde F, Laugier E, Santoni V, Hem S, Martin A, Gojon A, Schulze W, Lejay L. 2020. NRT2.1 phosphorylation prevents root high affinity nitrate uptake activity in Arabidopsis thaliana. *New Phytologist,* **228**, 1038-1054.
Kiba T, Feria-Bourrellier A-B, Lafouge F, Lezhnev L, Boutet-Mercey S, Orsel M, Bréhaut V, Miller A, Daniel-Vedele F, Sakakibara H, Krapp A. 2012. The Arabidopsis nitrate transporter NRT2.4 plays a double role in roots and shoots of nitrogen-starved plants. *The Plant Cell* **24**, 245-258.
Krapp A, David LC, Chardin C, Girin T, Marmagne A, Leprince AS, Chaillou S, Ferrario-Mery S, Meyer C, Daniel-Vedele F. 2014. Nitrate transport and signalling in Arabidopsis. *Journal of Experimental Botany* **65**, 789-798.
Krouk G, Crawford NM, Coruzzi GM, Tsay YF. 2010. Nitrate signaling: adaptation to fluctuating environments. *Current Opinion in Plant Biology* **13**, 266-273.
Laohavisit A, Wakatake T, Ishihama N, Mulvey H, Takizawa K, Suzuki T, Shirasu K. 2020. Quinone perception in plants via leucine-rich-repeat receptor-like kinases. *Nature* **587**, 92-97.
Laugier E, Bouguyon E, Mauriès A, Tillard P, Gojon A, Lejay L. 2012. Regulation of high-affinity nitrate uptake in roots of Arabidopsis depends predominantly on posttranscriptional control of the NRT2.1/NAR2.1 transport system. *Plant Physiology* **158**, 1067-1078.
Lejay L, Gansel X, Cerezo M, Tillard P, Müller C, Krapp A, von Wirén N, Daniel-Vedele F, Gojon A. 2003. Regulation of root ion transporters by photosynthesis: Functional importance and relation with hexokinase. *The Plant Cell* **15**, 2218-2232.
Lejay L, Tillard P, Domingo-Olive F, Lepetit M, Olive FD, Filleur S, Daniel-Vedele F, Gojon A. 1999. Molecular and functional regulation of two NO3-uptake systems by N- and C-status of Arabidopsis plants. *Plant Journal* **18**.
Leran S, Varala K, Boyer JC, Chiurazzi M, Crawford N, Daniel-Vedele F, David L, Dickstein R, Fernandez E, Forde B, Gassmann W, Geiger D, Gojon A, Gong JM, Halkier BA, Harris JM, Hedrich R, Limami AM, Rentsch D, Seo M, Tsay YF, Zhang M, Coruzzi G, Lacombe B. 2014. A unified nomenclature of NITRATE TRANSPORTER 1/PEPTIDE TRANSPORTER family members in plants. *Trends in Plant Science* **19**, 5-9.
Li G, Tillard P, Gojon A, Maurel C. 2016. Dual regulation of root hydraulic conductivity and plasma membrane aquaporins by plant nitrate accumulation and high-affinity nitrate transporter NRT2.1. *Plant and Cell Physiology* **57**, 733-742.

Liu KH, Huang CY, Tsay YF. 1999. CHL1 is a dual-affinity nitrate transporter of Arabidopsis involved in multiple phases of nitrate uptake. *The Plant Cell* **11**, 865-874.
Liu KH, Tsay YF. 2003. Switching between the two action modes of the dual-affinity nitrate transporter CHL1 by phosphorylation. *EMBO Journal* **22**, 1005-1013.
Menz J, Li Z, Schulze W, Ludewig U. 2016. Early nitrogen-deprivation responses in Arabidopsis roots reveal distinct differences on transcriptome and (phospho-) proteome levels between nitrate and ammonium nutrition. *The Plant Journal* **88**, 717-734.
Mitchell AL, Attwood TK, Babbitt PC, Blum M, Bork P, Bridge A, Brown SD, Chang HY, El-Gebali S, Fraser MI, Gough J, Haft DR, Huang H, Letunic I, Lopez R, Luciani A, Madeira F, Marchler-Bauer A, Mi H, Natale DA, Necci M, Nuka G, Orengo C, Pandurangan AP, Paysan-Lafosse T, Pesseat S, Potter SC, Qureshi MA, Rawlings ND, Redaschi N, Richardson LJ, Rivoire C, Salazar GA, Sangrador-Vegas A, Sigrist CJA, Sillitoe I, Sutton GG, Thanki N, Thomas PD, Tosatto SCE, Yong SY, Finn RD. 2019. InterPro in 2019: improving coverage, classification and access to protein sequence annotations. *Nucleic Acids Research* **47**, D351-D360.
Nolen B, Taylor S, Ghosh G. 2004. Regulation of protein kinases; controlling activity through activation segment conformation. *Molecular Cell* **15**, 661-675.
Ohkubo Y, Kuwata K, Matsubayashi Y. 2021. A type 2C protein phosphatase activates high-affinity nitrate uptake by dephosphorylating NRT2.1. *Nature Plants* **7**, 310-316.
Orsel M, Chopin F, Leleu O, Smith SJ, Krapp A, Daniel-Vedele F, Miller AJ. 2006. Characterization of a two-component high-affinity nitrate uptake system in Arabidopsis. Physiology and protein-protein interaction. *Plant Physiology* **143**, 1304-1317.
Orsel M, Chopin F, Leleu O, Smith SJ, Krapp A, Vedele FD, Miller AJ. 2007. Nitrate signaling and the two component high affinity uptake system in Arabidopsis. *Plant Signaling and Behaviour* **2**, 260-262.
Parker JL, Newstead S. 2014. Molecular basis of nitrate uptake by the plant nitrate transporter NRT1.1. *Nature* **507**, 68-72.
Perraki A, DeFalco TA, Derbyshire P, Avila J, Sere D, Sklenar J, Qi X, Stransfeld L, Schwessinger B, Kadota Y, Macho AP, Jiang S, Couto D, Torii KU, Menke FLH, Zipfel C. 2018. Phosphocode-dependent functional dichotomy of a common co-receptor in plant signalling. *Nature* **561**, 248-252.
Pertl H, Himly M, Gehwolf R, Kriechbaumer R, Strasser D, Michalke W, Richter K, Ferreira F, Obermeyer G. 2001. Molecular and physiological characterisation of a 14-3-3 protein from lily pollen grains regulating the activity of the plasma membrane H+ ATPase during pollen grain germination and tube growth. *Planta* **213**, 132-141.
Rodriguez MC, Petersen M, Mundy J. 2010. Mitogen-activated protein kinase signaling in plants. *Annual Review of Plant Biology* **61**, 621-649.
Rudashevskaya EL, Ye J, Jensen ON, Fuglsang AT, Palmgren MG. 2012. Phosphosite mapping of P-type plasma membrane H+-ATPase in homologous and heterologous environments. *Journal of Biological Chemistry* **287**, 4904-4913.
Schindelin J, Arganda-Carreras I, Frise E, Kaynig V, Longair M, Pietzsch T, Preibisch S, Rueden C, Saalfeld S, Schmid B, Tinevez JY, White DJ, Hartenstein V, Eliceiri K, Tomancak P, Cardona A. 2012. Fiji: an open-source platform for biological-image analysis. *Nat Methods* **9**, 676-682.
Schultz J, Milpertz F, Bork P, Ponting CP. 1998. SMART, a simple modular architecture research tool: Identification of signaling domains. *Proceedings of the National Academy of Sciences of the USA* **95**, 5857-5864.
Tan YZ, Keon KA, Abdelaziz R, Imming P, Schulze W, Schumacher K, Rubinstein JL. 2022. Structure of V-ATPase from citrus fruit. *Structure* **30**, 1403-1410 e1404.
Tanz SK, Castleden I, Hooper CM, Vacher M, Small I, Millar HA. 2013. SUBA3: a database for integrating experimentation and prediction to define the SUBcellular location of proteins in Arabidopsis. *Nucleic Acids Research* **41**, D1185-1191.

Thimm O, Bläsing O, Gibon Y, Nagel A, Meyer S, Kruger P, Selbig J, Muller LA, Rhee SY, Stitt M. 2004. MAPMAN: a user-driven tool to display genomics data sets onto diagrams of metabolic pathways and other biological processes. *The Plant Journal* **37**, 914-939.
Tyanova S, Temu T, Sinitcyn P, Carlson A, Hein MY, Geiger T, Mann M, Cox J. 2016. The Perseus computational platform for comprehensive analysis of (prote)omics data. *Nature Methods* **13**, 731-740.
Wang X, Bian Y, Cheng K, Gu L-F, Ye M, Zou H, He J-X. 2013. A large-scale protein phosphorylation analysis reveals novel phosphorylation motifs and phosphoregulatory networks in Arabidopsis. *Journal of Proteomics* **14**, 486-498.
Wang YY, Hsu PK, Tsay YF. 2012. Uptake, allocation and signaling of nitrate. *Trends in Plant Science* **17**, 458-467.
Wingenter K, Trentmann O, Winschuh I, Hörmiller II, Heyer AG, Reinders J, Schulz A, Geiger D, Hedrich R, H.E. N. 2011. A member of the mitogen-activated protein 3-kinase family is involved in the regulation of plant vacuolar glucose uptake. *Plant Journal* **68**, 890-900.
Winter D, Vinegar B, Nahal H, Ammar R, Wilson GV, Provart NJ. 2007. An "electronic fluorescent pictograph" browser for exploring and analyzing large-scale biological data sets. *PLoS ONE* **2**, e718.
Wirth J, Chopin F, Santoni V, Viennois G, Tillard P, Krapp A, Lejay L, Daniel-Vedele F, Gojon A. 2007. Regulation of root nitrate uptake at the NRT2.1 protein level in Arabidopsis thaliana. *Journal of Biological Chemistry* **282**, 23541-23552.
Wu F, Chi Y, Jiang Z, Xu Y, Xie L, Huang F, Wan D, Ni J, Yuan F, Wu X, Zhang Y, Wang L, Ye R, Byeon B, Wang W, Zhang S, Sima M, Chen S, Zhu M, Pei J, Johnson DM, Zhu S, Cao X, Pei C, Zai Z, Liu Y, Liu T, Swift GB, Zhang W, Yu M, Hu Z, Siedow JN, Chen X, Pei ZM. 2020. Hydrogen peroxide sensor HPCA1 is an LRR receptor kinase in Arabidopsis. *Nature* **578**, 577-581.
Wu X, Liu T, Zhang Y, Duan F, Neuhauser B, Ludewig U, Schulze WX, Yuan L. 2019a. Ammonium and nitrate regulate NH4+ uptake activity of Arabidopsis ammonium transporter AtAMT1;3 via phosphorylation at multiple C-terminal sites. *Journal of Experimental Botany* **70**, 4919-4930.
Wu XN, Chu L, Xi L, Pertl-Obermeyer H, Li Z, Sklodowski K, Sanchez-Rodriguez C, Obermeyer G, Schulze WX. 2019b. Sucrose-induced Receptor Kinase 1 is Modulated by an Interacting Kinase with Short Extracellular Domain. *Molecular and Cellular Proteomics* **18**, 1556-1571.
Wu XN, Schulze WX. 2015. Kinase activity and specificity assay using synthetic peptides. *Methods in Molecular Biology* **1306**, 97-104.
Wu XN, Xi L, Pertl-Obermeyer H, Li Z, Chu LC, Schulze WX. 2017. Highly Efficient Single-Step Enrichment of Low Abundance Phosphopeptides from Plant Membrane Preparations. *Frontiers in Plant Science* **8**, 1673.
Yong Z, Kotur Z, Glass AD. 2010. Characterization of an intact two-component high-affinity nitrate transporter from Arabidopsis roots. *The Plant Journal* **63**, 739-748.
Zauber H, Schulze WX. 2012. Proteomics wants cRacker: Automated standardized data analysis of LC/MS derived proteomic data. *Journal of Proteome Research* **11**, 5548-5555.
Zou X, Liu M, Wu W, Wang Y. 2019. Phosphorylaiton at Ser28 stabilizes the Arabidopsis nitrate transporter NRT2.1 in response to nitrate limitation. *Journal of Integrative Plant Biology*.
Zulawski M, Schulze WX. 2015. The plant kinome. *Methods in Molecular Biology* **1306**, 1-23.

Figures Legends

Figure 1: Regulation of nitrate uptake by N-terminal NRT2.1 phosphorylation at (**A**) S11, (**B**) S28, (**C**) and S21. In all panels, wild type and *nrt2.1* knock out mutant were used as controls. Phosphorylation site mutants of *NRT2.1* were expressed under the *NRT2.1* promoter in the *nrt2.1* mutant background as phosphomimicking (S to D) or phosphodead (S to A) version of different phosphorylation sites. Bars of same color indicate independent lines expressing the same construct (S to D, or S to A). Averages with standard deviation are displayed, asterisks indicate significant differences to wild type within one treatment (*** $p<0.001$, ** $p<0.01$, * $p<0.05$, pairwise t-test). Dots indicate average uptake rates of different plant lines expressing S to D or S to A mutants. Letters indicate significant differences ($p<0.05$, pairwise t-test) between phosphomimicking and phosphodead mutants within each treatment.

Figure 2: Interaction of NRT2.1 with NAR2.1. (**A**) The effect of phosphodead (S to A) and phosphomimicking (S to D) mutations of NRT2.1 single phosphorylation site mutations on the interaction with NAR2.1. (**B**) The effect of double phosphorylation site mutations at S21 and S28 on the interaction with NAR2.1. Numbers indicate the total number of cells quantified. Small letters indicate significant differences as determined by pairwise rank sum test ($p<0.05$). Higher YFP/RFP ratio indicate stronger interaction.

Figure 3: Phosphorylation and interaction network of NRT2.1 and its putative kinases (**A**) Correlation network of NRT2.1 phosphorylation sites S11, S28, S501 and T521 with plasma membrane located kinases under nitrate deprivation and nitrate resupply with 5 mM and 0.2 mM NO_3^-. Solid edges: positive correlation, dashed edges: negative correlation. Edge color: black, 5mM NO_3^-; gray, 0.2 mM NO_3^-; light gray, nitrogen deprivation. Node color: blue, receptor kinases; light blue, calcium signaling; gray, other kinases. (**B**) Interaction network of NRT2.1 and the selected putative kinase AT5G49770 extended by known experimentally confirmed interaction partners from STRING (Franceschini *et al.*, 2013). Node color: red, transport proteins; blue, signaling proteins; yellow, nitrogen metabolism, pink: other.

Figure 4: Kinase AT5G49770 interacts with and phosphorylates NRT2.1 at S21. (**A**) The effect of phosphodead (S to A) and phosphomimicking (S to D) mutations of AT5G49770 phosphorylation sites on the interaction with NRT2.1. Numbers indicate the total number of cells quantified. Small letters indicate significant differences as determined by pairwise rank sum test ($p<0.05$). (**B**) *In vitro* kinase activity assay using the NRT2.1 peptide EQSFAFSVQSPIVHTDK as a substrate. Averages with standard deviations are displayed, small letters indicates significant differences based on pairwise t-test ($p<0.05$). Dotted bars denote phosphorylation site S839. Domain model of the AT5G49770 kinase based on SMART is displayed as insert (Schultz *et al.*, 1998). (**C**) Representative fragment spectrum of *in vitro* kinase activity assay showing specific phosphorylation of the substrate peptide EQSFAFSVQSPIVHTDK at S21. Spectrum was directly exported from MaxQuant version 1.5.3.30 (Cox and Mann, 2008). (**D**) *In vitro* kinase activity assay using myelin basic protein as a substrate. Averages with standard deviations are displayed, small letters indicates significant differences based on pairwise t-test ($p<0.05$).

Figure 5: Phosphorylation status of NRT2.1 S21, S28 and AT5G49770 S870, S839 under different nutritional context. Results present the abundance of individual phosphopeptides and cannot conclude about phosphorylation combinations of individual NRT2.1 molecules. (**A**) Phosphorylation

of NRT2.1 at S21. (**B**) Phosphorylation of NRT2.1 at S28. (**C**) Phosphorylation of AT5G49770 at S870, (**D**) Phosphorylation of AT5G49770 at S839. In panels (A) to (D) raw files from previous experiments (Engelsberger and Schulze, 2012; Menz *et al.*, 2016) and current experiment of resupply with 0.2 mM and 5 mM nitrate were processed together and quantified. Average normalized ion intensity values of three biological replicates are shown with standard deviation as determined by cRacker (Zauber and Schulze, 2012). ND: not detected. (**E**) Interaction of AT5G49770 with NRT2.1 and respective NRT2.1 phosphorylation site mutants as determined from ratiometric bimolecular fluorescence experiments. Numbers indicate the number of quantified cells. In all panels small letters indicate significant differences as derived from a ONEWAY-ANOVA analysis ($p<0.05$).

Figure 6: Interaction of AT5G49770 with NRT2.1 phosphorylation site mutants and nitrate uptake of kinase knock-out. (**A**) Nitrate influx rate of wild type, *nrt2.1* knock-out and *at5g49770* knock-out under nitrate starvation (-N) and induction with 1 mM nitrate for 4 hours and 7 hours. Averages (n=4) with standard deviations are shown. (**B**) Expression of *NRT2.1* (**C**) *NAR2.1* mRNA and (**D**) *At5g49770* mRNA in wild type, *nrt2.1* knock-out and *at5g49770* knock-out mutant. Averages of three biological replicates are shown with standard deviation, asterisks indicate significant differences to wild type within one treatment (*** $p<0.001$, ** $p<0.01$, * $p<0.05$, pairwise t-test).

Figure 7: Functional model of NRT2.1 regulation at the N-terminus involving two single phosphorylated states NRT2.1 at S21 and S28 under conditions of induction by 1mM nitrate for 4 hours. NAR2.1 is shown in green and kinase HPCAL1 is shown in yellow. Functional relevance of other N- and C-terminal NRT2.1 phosphorylation sites was not considered in this figure.

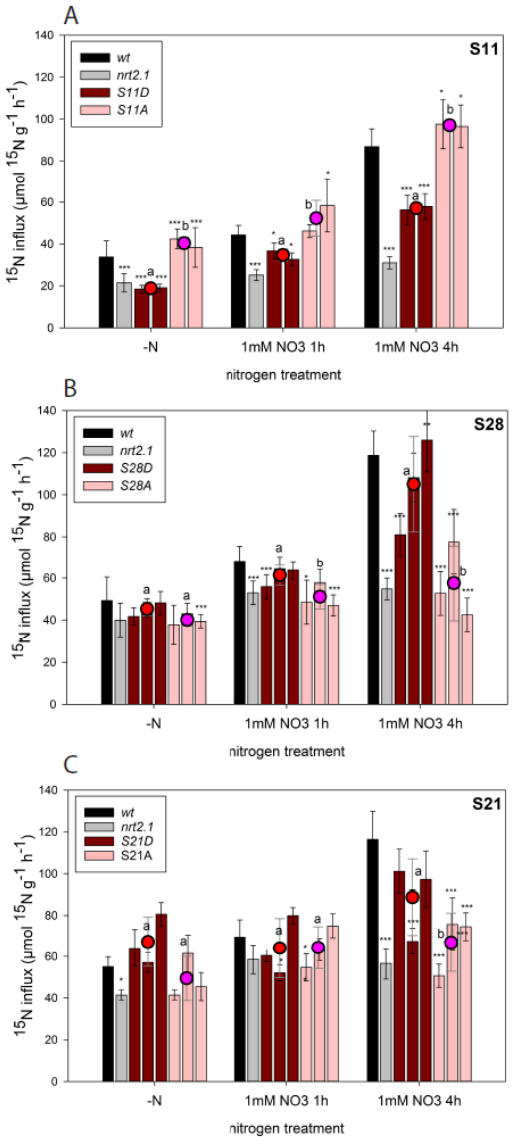

Figure 1: Regulation of nitrate uptake by N-terminal NRT2.1 phosphorylation at (**A**) S11, (**B**) S28, (**C**) and S21. In all panels, wild type and *nrt2.1* knock out mutant were used as controls. Phosphorylation site mutants of *NRT2.1* were expressed under the *NRT2.1* promoter in the *nrt2.1* mutant background as phosphomimicking (S to D) or phosphodead (S to A) version of different phosphorylation sites. Bars of same color indicate independent lines expressing the same construct (S to D, or S to A). Averages with standard deviation are displayed, asterisks indicate significant differences to wild type within one treatment (*** p<0.001, ** p<0.01, * p<0.05, pairwise t-test). Dots indicate average uptake rates of different plant lines expressing S to D or S to A mutants. Letters indicate significant differences (p<0.05, pairwise t-test) between phosphomimicking and phosphodead mutants within each treatment.

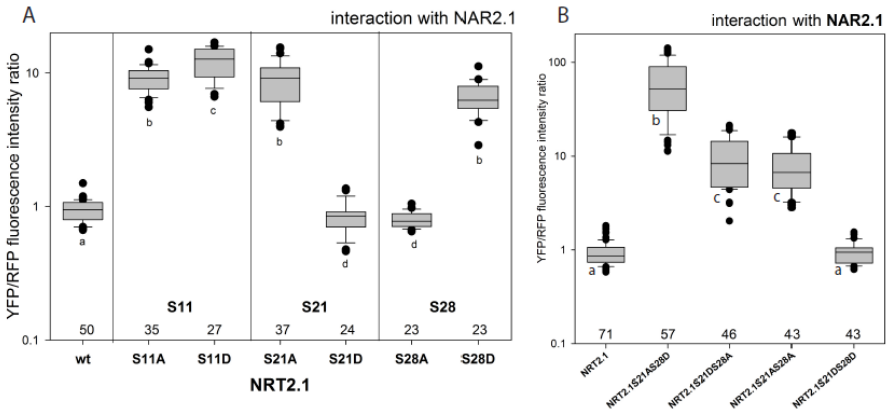

Figure 2: Interaction of NRT2.1 with NAR2.1. (**A**) The effect of phosphodead (S to A) and phosphomimicking (S to D) mutations of NRT2.1 single phosphorylation site mutations on the interaction with NAR2.1. (**B**) The effect of double phosphorylation site mutations at S21 and S28 on the interaction with NAR2.1. Numbers indicate the total number of cells quantified. Small letters indicate significant differences as determined by pairwise rank sum test ($p<0.05$). Higher YFP/RFP ratio indicate stronger interaction.

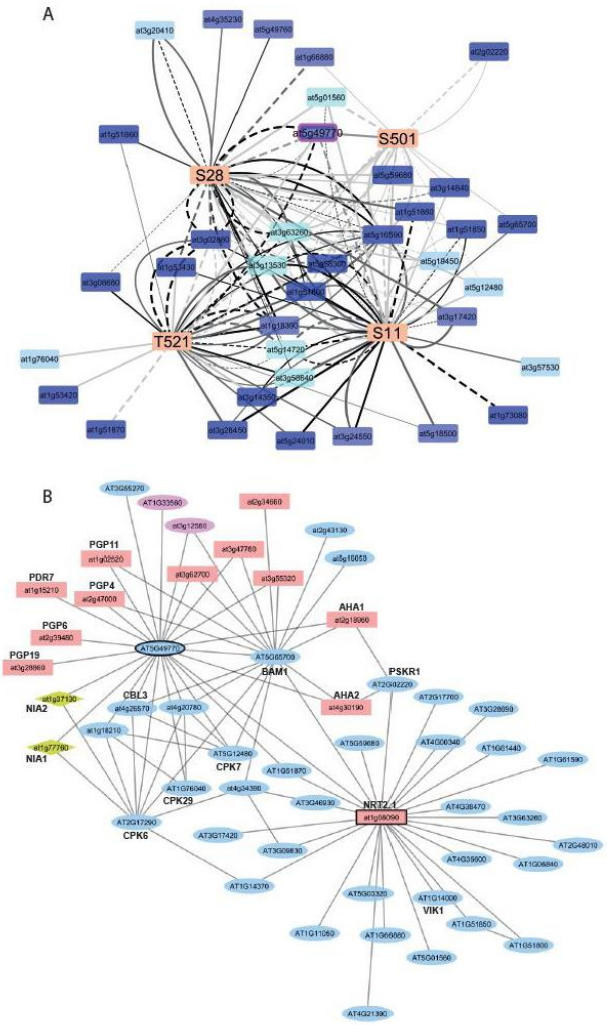

Figure 3: Phosphorylation and interaction network of NRT2.1 and its putative kinases (**A**) Correlation network of NRT2.1 phosphorylation sites S11, S28, S501 and T521 with plasma membrane located kinases under nitrate deprivation and nitrate resupply with 5 mM and 0.2 mM NO_3^-. Solid edges: positive correlation, dashed edges: negative correlation. Edge color: black, 5mM NO_3^-; gray, 0.2 mM NO_3^-; light gray, nitrogen deprivation. Node color: blue, receptor kinases; light blue, calcium signaling; gray, other kinases. (**B**) Interaction network of NRT2.1 and the selected putative kinase AT5G49770 extended by known experimentally confirmed interaction partners from STRING (Franceschini *et al.*, 2013). Node color: red, transport proteins; blue, signaling proteins; yellow, nitrogen metabolism, pink: other.

Franceschini A, Szklarczyk D, Frankild S, Kuhn M, Simonovic M, Roth A, Lin J, Minguez P, Bork P, Von Mering C, Jensen LJ. 2013. STRING v9.1: protein-protein interaction networks, with increased coverage and integration. *Nucleic Acids Research* **41**, D808-D815.

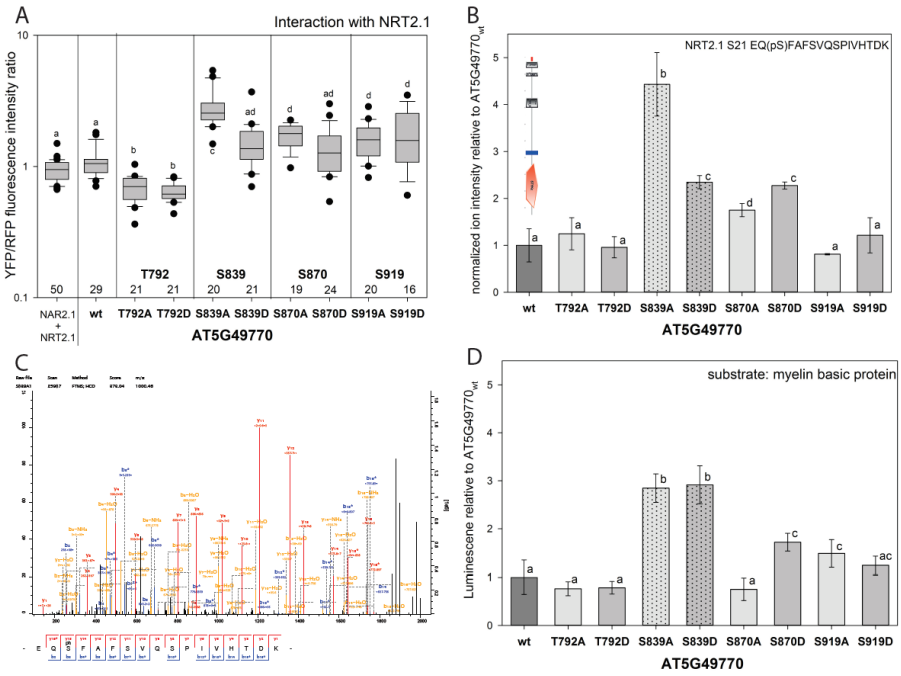

Figure 4: Kinase AT5G49770 interacts with and phosphorylates NRT2.1 at S21. (**A**) The effect of phosphodead (S to A) and phosphomimicking (S to D) mutations of AT5G49770 phosphorylation sites on the interaction with NRT2.1. Numbers indicate the total number of cells quantified. Small letters indicate significant differences as determined by pairwise rank sum test ($p<0.05$). (**B**) *In vitro* kinase activity assay using the NRT2.1 peptide EQSFAFSVQSPIVHTDK as a substrate. Averages with standard deviations are displayed, small letters indicates significant differences based on pairwise t-test ($p<0.05$). Dotted bars denote phosphorylation site S839. Domain model of the AT5G49770 kinase based on SMART is displayed as insert (Schultz *et al.*, 1998). (**C**) Representative fragment spectrum of *in vitro* kinase activity assay showing specific phosphorylation of the substrate peptide EQSFAFSVQSPIVHTDK at S21. Spectrum was directly exported from MaxQuant version 1.5.3.30 (Cox and Mann, 2008). (**D**) *In vitro* kinase activity assay using myelin basic protein as a substrate. Averages with standard deviations are displayed, small letters indicates significant differences based on pairwise t-test ($p<0.05$).

Cox J, Mann M. 2008. MaxQuant enables high peptide identification rates, individualized p.p.b.-range mass accuracies and proteome-wide protein quantification. *Nature Biotechnology* **26**, 1367-1372.
Schultz J, Milpertz F, Bork P, Ponting CP. 1998. SMART, a simple modular architecture research tool: Identification of signaling domains. *Proceedings of the National Academy of Sciences of the USA* **95**, 5857-5864.

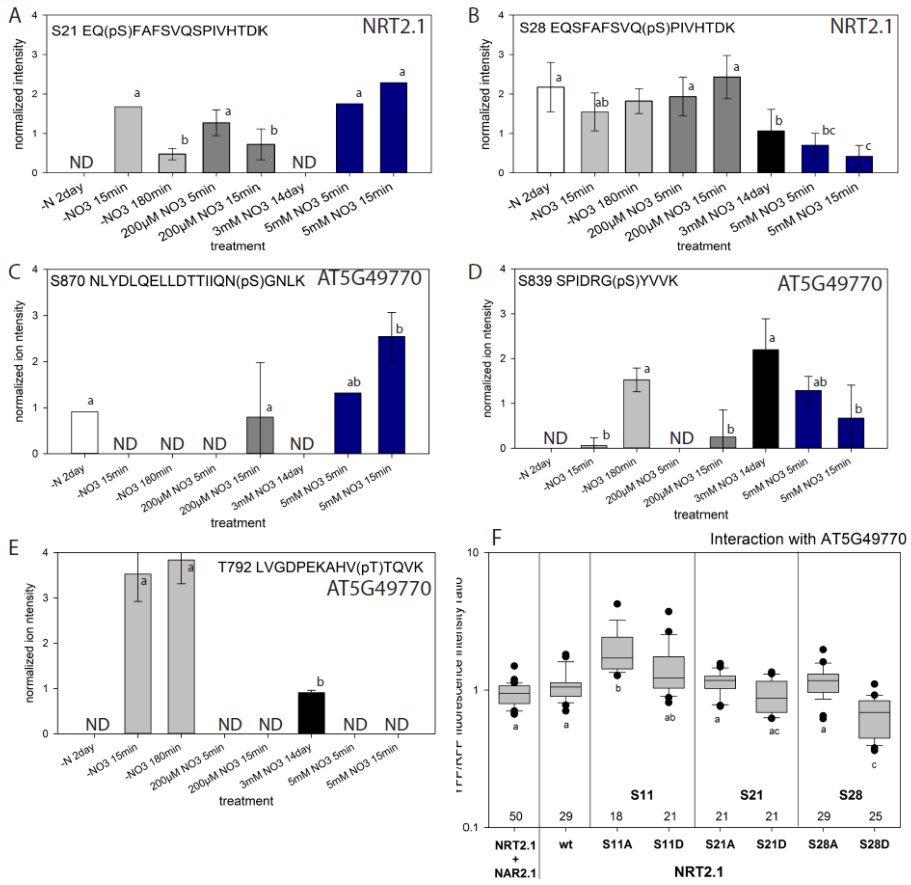

Figure 5: Phosphorylation status of NRT2.1 S21, S28 and AT5G49770 S870, S839 under different nutritional context. Results present the abundance of individual phosphopeptides and cannot conclude about phosphorylation combinations of individual NRT2.1 molecules. (**A**) Phosphorylation of NRT2.1 at S21. (**B**) Phosphorylation of NRT2.1 at S28. (**C**) Phosphorylation of AT5G49770 at S870, (**D**) Phosphorylation of AT5G49770 at S839. In panels (A) to (D) raw files from previous experiments (Engelsberger and Schulze, 2012; Menz *et al.*, 2016) and current experiment of resupply with 0.2 mM and 5 mM nitrate were processed together and quantified. Average normalized ion intensity values of three biological replicates are shown with standard deviation as determined by cRacker (Zauber and Schulze, 2012). ND: not detected. (**E**) Interaction of AT5G49770 with NRT2.1 and respective NRT2.1 phosphorylation site mutants as determined from ratiometric bimolecular fluorescence experiments. Numbers indicate the number of quantified cells. In all panels small letters indicate significant differences as derived from a ONEWAY-ANOVA analysis ($p<0.05$).

Engelsberger WR, Schulze WX. 2012. Nitrate and ammonium lead to distinct global dynamic phosphorylation patterns when resupplied to nitrogen starved Arabidopsis seedlings. *The Plant Journal* **69**, 978-995.
Menz J, Li Z, Schulze W, Ludewig U. 2016. Early nitrogen-deprivation responses in Arabidopsis roots reveal distinct differences on transcriptome and (phospho-) proteome levels between nitrate and ammonium nutrition. *The Plant Journal* **88**, 717-734.
Zauber H, Schulze WX. 2012. Proteomics wants cRacker: Automated standardized data analysis of LC/MS derived proteomic data. *Journal of Proteome Research* **11**, 5548-5555.

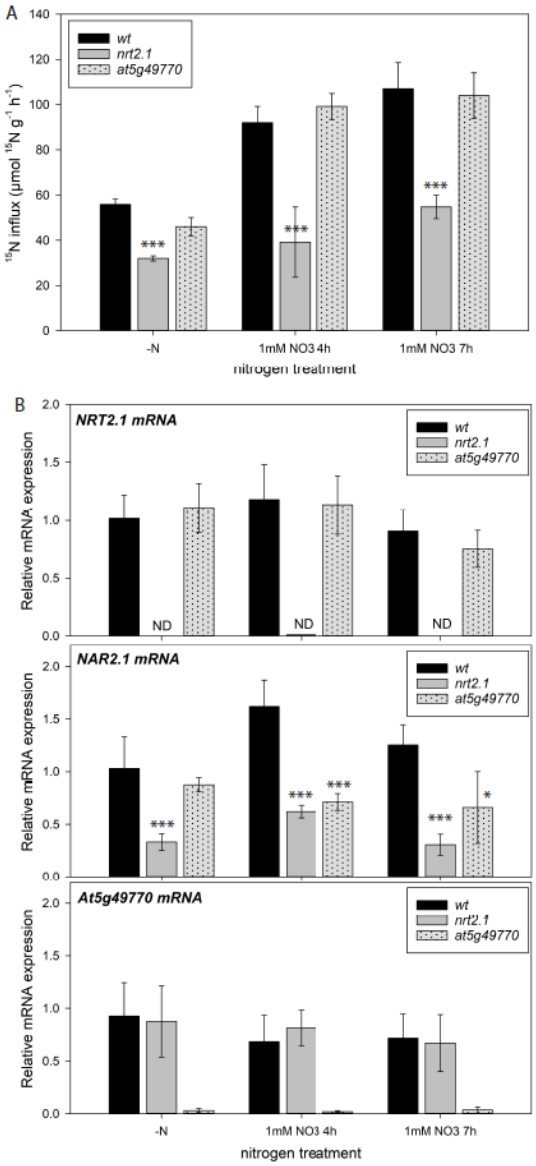

Figure 6: Interaction of AT5G49770 with NRT2.1 phosphorylation site mutants and nitrate uptake of kinase knock-out. (**A**) Nitrate influx rate of wild type, *nrt2.1* knock-out and *at5g49770* knock-out under nitrate starvation (-N) and induction with 1 mM nitrate for 4 hours and 7 hours. Averages (n=4) with standard deviations are shown. (**B**) Expression of *NRT2.1* (**C**) *NAR2.1* mRNA and (**D**) *At5g49770* mRNA in wild type, *nrt2.1* knock-out and *at5g49770* knock-out mutant. Averages of three biological replicates are shown with standard deviation, asterisks indicate significant differences to wild type within one treatment (*** p<0.001, ** p<0.01, * p<0.05, pairwise t-test).

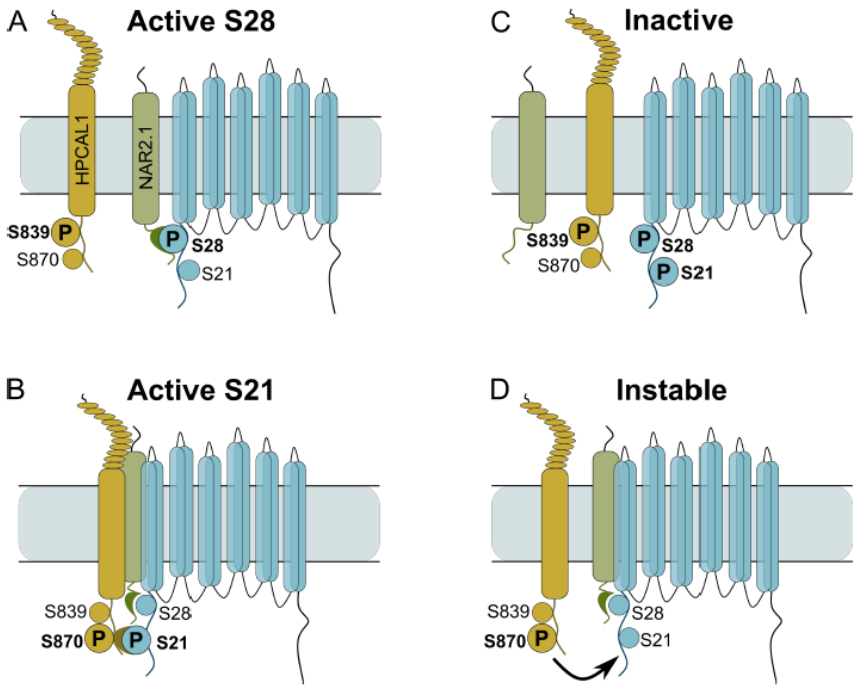

Figure 7: Functional model of NRT2.1 regulation at the N-terminus involving two single phosphorylated states NRT2.1 at S21 and S28 under conditions of induction by 1mM nitrate for 4 hours. NAR2.1 is shown in green and kinase HPCAL1 is shown in yellow. Functional relevance of other N- and C-terminal NRT2.1 phosphorylation sites was not considered in this figure.